THE JOURNAL OF PHYSICAL CHEMISTRY Letters

Letter

Cite This: J. Phys. Chem. Lett. 2018, 9, 895−901

pubs.acs.org/JPCL

Investigating the Role of the Organic Cation in Formamidinium Lead Iodide Perovskite Using Ultrafast Spectroscopy

Victoria C. A. Taylor,[†,‡] Devendra Tiwari,[*,†] Marta Duchi,[†] Paul M. Donaldson,[§] Ian P. Clark,[§] David J. Fermin,[†,‡] and Thomas A. A. Oliver[*,†,‡]

[†]School of Chemistry, University of Bristol, Bristol, BS8 1TS, United Kingdom

[‡]Bristol Centre for Functional Nanomaterials, University of Bristol, Bristol, BS8 1TL, United Kingdom

[§]Central Laser Facility, Science and Technology Facilities Council, Research Complex at Harwell, Rutherford Appleton Laboratory, Didcot, Oxfordshire OX11 0QX, United Kingdom

Supporting Information

ABSTRACT: Organic cation rotation in hybrid organic−inorganic lead halide perovskites has previously been associated with low charge recombination rates and (anti)ferroelectric domain formation. Two-dimensional infrared spectroscopy (2DIR) was used to directly measure 470 ± 50 fs and 2.8 ± 0.5 ps time constants associated with the reorientation of formamidinium cations (FA^+, $NH_2CHNH_2^+$) in formamidinium lead iodide perovskite thin films. Molecular dynamics simulations reveal the FA^+ agitates about an equilibrium position, with NH_2 groups pointing at opposite faces of the inorganic lattice cube, and undergoes 90° flips on picosecond time scales. Time-resolved infrared measurements revealed a prominent vibrational transient feature arising from a vibrational Stark shift: photogenerated charge carriers increase the internal electric field of perovskite thin films, perturbing the FA^+ antisymmetric stretching vibrational potential, resulting in an observed 5 cm^{-1} shift. Our 2DIR results provide the first direct measurement of FA^+ rotation inside thin perovskite films, and cast significant doubt on the presence of long-lived (anti)ferroelectric domains, which the observed low charge recombination rates have been attributed to.

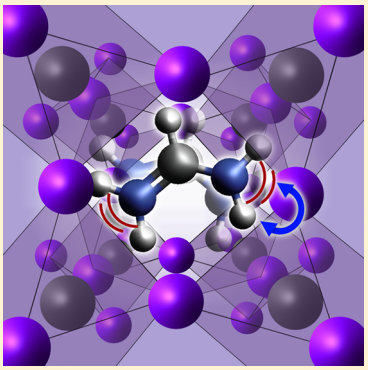

Hybrid organic−inorganic perovskites have found recent prominence as the active photovoltaic layer in optoelectronic devices due to high and balanced charge carrier mobilities,[1] tunable bandgaps,[2] and high absorption cross sections.[3] Perovskite films are cheap to synthesize using solution processing techniques, with functionality seemingly unimpaired by impurities, unlike competing semiconductors.[4] In addition to photovoltaics, perovskites have shown great promise for applications ranging from lasers,[5] photodetectors,[6] light-emitting devices,[7] thin film transistors[8] to spintronics.[9] Despite intense research efforts to enhance these promising attributes,[3,10−17] an underlying mechanistic understanding of these highly desirable properties remains nebulous.

Organic lead iodide perovskites take the stoichiometry $APbI_3$, where A is an organic cation. In an ideal cubic perovskite crystal structure, the organic cation is caged within an inorganic lattice comprised of a cube of lead cations with an iodide octahedron around each lead cation. Despite a simple chemical structure, hybrid inorganic−organic lead halide perovskites have been shown to be inherently complex materials that support a diverse range of dynamical processes essential to their photovoltaic performance. These phenomena operate over a multitude of time scales and include organic and inorganic ion diffusion,[18] organic cation rotation,[14,15,19,20] and octahedral distortions.[17,21] Recent studies, however, indicate that static effects such as Rashba splitting in the conduction band, may play a pivotal role.[9,22]

The choice of organic cation in lead halide perovskites is significant, and can change the most stable phase at room temperature (e.g., orthorhombic vs tetragonal), resulting in different band gap energies.[2,21,23,24] Whether this arises from purely steric effects and changes to the lead iodide lattice spacing, or instead via changes in electronic structure induced by different van der Waals interactions between the cation and surrounding inorganic lattice, is a matter of controversy.[25−27] Several prominent studies have proposed that the rapid reorientation and/or alignment of organic cations may be a crucial factor contributing toward the observed low charge recombination rates for hybrid perovskites.[1,16,24,28] The proposed mechanisms involve either (i) photoexcited charge carriers causing proximal cations to reorient, inducing fluctuations and distortions in the inorganic lattice through van der Waals electrostatic interactions and the formation of large polarons;[20,27,29,30] or (ii) neighboring organic cation dipoles aligning to form (anti)ferroelectric domains, which can channel opposite charges away from each other via the

Received: December 13, 2017
Accepted: February 1, 2018
Published: February 1, 2018

DOI: 10.1021/acs.jpclett.7b03296
J. Phys. Chem. Lett. 2018, 9, 895−901

boundaries of such domains.[24,28,31,32] Studies of the hybrid perovskite archetype, methylammonium lead iodide perovskite ($MAPbI_3$), revealed that the organic cation reorients on the order of several picoseconds at room temperature.[12,14,15,19]

Some of the latest hybrid lead halide perovskite thin films use formamidinium ($NH_2CHNH_2^+$, FA^+) as the organic cation. This results in a favorable red-shift toward the ideal band gap.[33] A recent study examining the carrier diffusion length of single crystals, indicated that many lead-halide (Br, I) perovskites incorporating FA^+ display increased carrier diffusion lengths by up to a factor of 4 (cf. methylammonium containing perovskites), which was attributed to ferroelectric domain formation.[1] Despite these promising photovoltaic properties, to date, experimental studies have yet to directly determine the presence of ferroelectric domains in formamidinium lead iodide perovskite ($FAPbI_3$) thin films, and make a direct connection between their promising photoactive properties and underlying molecular structure.

In this work, we investigate the vibrational dynamics associated with the formamidinium cation in $FAPbI_3$ films and elucidate the influence of the reorientation time scales of FA^+ on the photophysical material properties using two-dimensional vibrational spectroscopy (2DIR). Time-resolved infrared spectroscopy (TRIR) measurements were also used to probe the effect of photoinduced charges on the organic cation. We show, for the first time, that FA^+ reorientation is characterized by 470 ± 50 fs and 2.8 ± 0.5 ps time constants. Such rapid reorientation shows that ferroelectric domains are unlikely to play any role in long carrier lifetimes.

For infrared spectroscopic measurements, the strong mid-infrared peak centered at 1713 cm^{-1}, (see FTIR spectrum in Figure 1a) was used to probe the inorganic lattice−molecular cation interactions. This vibrational feature has previously been attributed to the C=N symmetric stretching vibration of the FA cation;[34,35] however, these studies did not include any justification for this assignment. We used high-level coupled cluster *ab initio* calculations with single and double excitations (CCSD) with an aug-cc-pVTZ basis set to calculate the normal modes and associated frequencies of the formamidinium cation. Our calculations show the 1713 cm^{-1} feature should instead be assigned to the C−N antisymmetric stretching vibration. The associated vibrational transition dipole moment lies in the plane of the molecule along an axis that lies parallel to the two nitrogen atoms (see Figure 1a). The details of $FAPbI_3$ thin film synthesis are given in the Supporting Information (SI). Linear absorption and fluorescence spectroscopy (Figure 1b) alongside X-ray diffraction measurements confirmed that $FAPbI_3$ thin films were present in the cubic (α) phase with Pm3m space group (see SI). We investigated the cation rotation in two different samples: $FAPbI_3$ thin films deposited on CaF_2 substrates, and $FAPbI_3$ thin films sandwiched between hole transport material spiro-OMeTAD and electron acceptor titanium dioxide. TRIR studies were only performed on $FAPbI_3$ thin films.

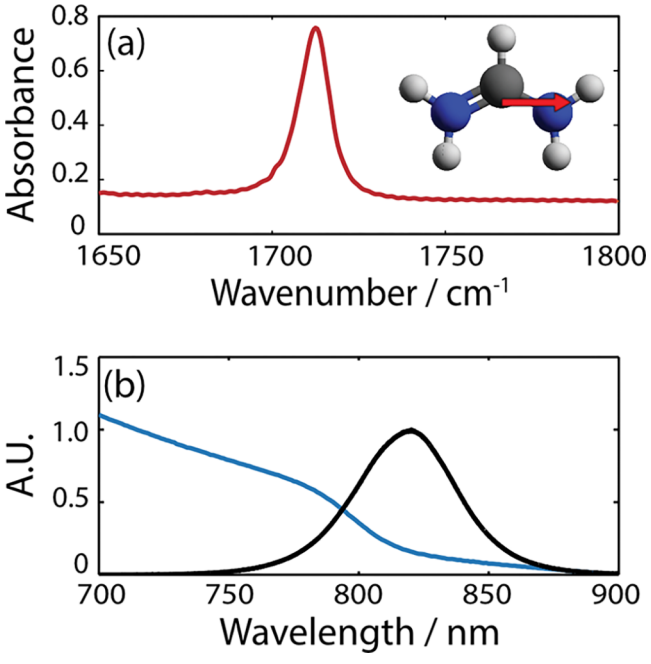

Figure 1. (a) Linear infrared absorption spectrum, and inset optimized CCSD/aug-cc-pVTZ structure of the FA^+ cation, with overlaid vibrational transition dipole moment for the C−N antisymmetric stretching vibration. (b) Linear electronic absorption (blue) and fluorescence spectra (black) for the $FAPbI_3$ sample used in this study.

Ground state 2DIR spectra were found to be contaminated with a thermal component, as previously reported for 2DIR studies of $MAPbI_3$ thin films.[12,14] Through a higher-order singular value decomposition, we were able to isolate and remove some part of these signals from the 2DIR spectra for data acquired in parallel and perpendicular pump−probe configurations (I_{para} and I_{perp}, respectively)- see SI for details of this procedure. We note that the thermal component is isotropic and therefore does not affect our anisotropy results (see Figure S9). These data were then used to generate isotropic 2DIR spectra through the relation

$$I_{iso}(t_2) = \frac{1}{3}(I_{para} + 2I_{perp}) \quad (1)$$

Figure 2 displays isotropic 2DIR spectra at four waiting times for FA^+. The spectra are dominated by two features; the negative feature centered on the diagonal (black dashed line) at 1713 cm^{-1} corresponds to overlapping ground state bleach (GSB) and stimulated emission (SE) signals associated with the C−N antisymmetric stretch of the FA^+ cation. The positive feature centered at ω_3 = 1706 cm^{-1} is the corresponding excited state absorption (ESA) signal.

The GSB/SE and ESA features are predominantly homogeneously broadened, i.e., the diagonal and antidiagonal line widths are very similar, and they evolve little within the 100 ps measurement window. Center line slope analysis of the GSB/SE feature showed that the feature's line shape is almost entirely time-invariant within the noise limit of the experiment (see SI), indicating minimal or no spectral diffusion. We explain the apparent lack of spectral diffusion later in the context of our anisotropy results.

Figure 3a displays the population relaxation dynamics (isotropic signal) of the FA^+ C−N antisymmetric stretch GSB/SE feature for the two perovskite films. The kinetics associated with the film coated directly onto the CaF_2 windows, and sandwiched between hole and electron transport materials are essentially identical, and could be fit to a biexponential decay with 2.8 ± 0.2 ps and 500 ± 155 ps time constants. The 2.8 ps lifetime is similar to the vibrational lifetimes measured for the symmetric N^+H_3 bending mode of MA^+ in $MAPbI_3$ films.[12,14] The source of the long-lived component is unclear, FA^+ cations buried in the bulk and at the surface of the film

DOI: 10.1021/acs.jpclett.7b03296
J. Phys. Chem. Lett. 2018, 9, 895−901

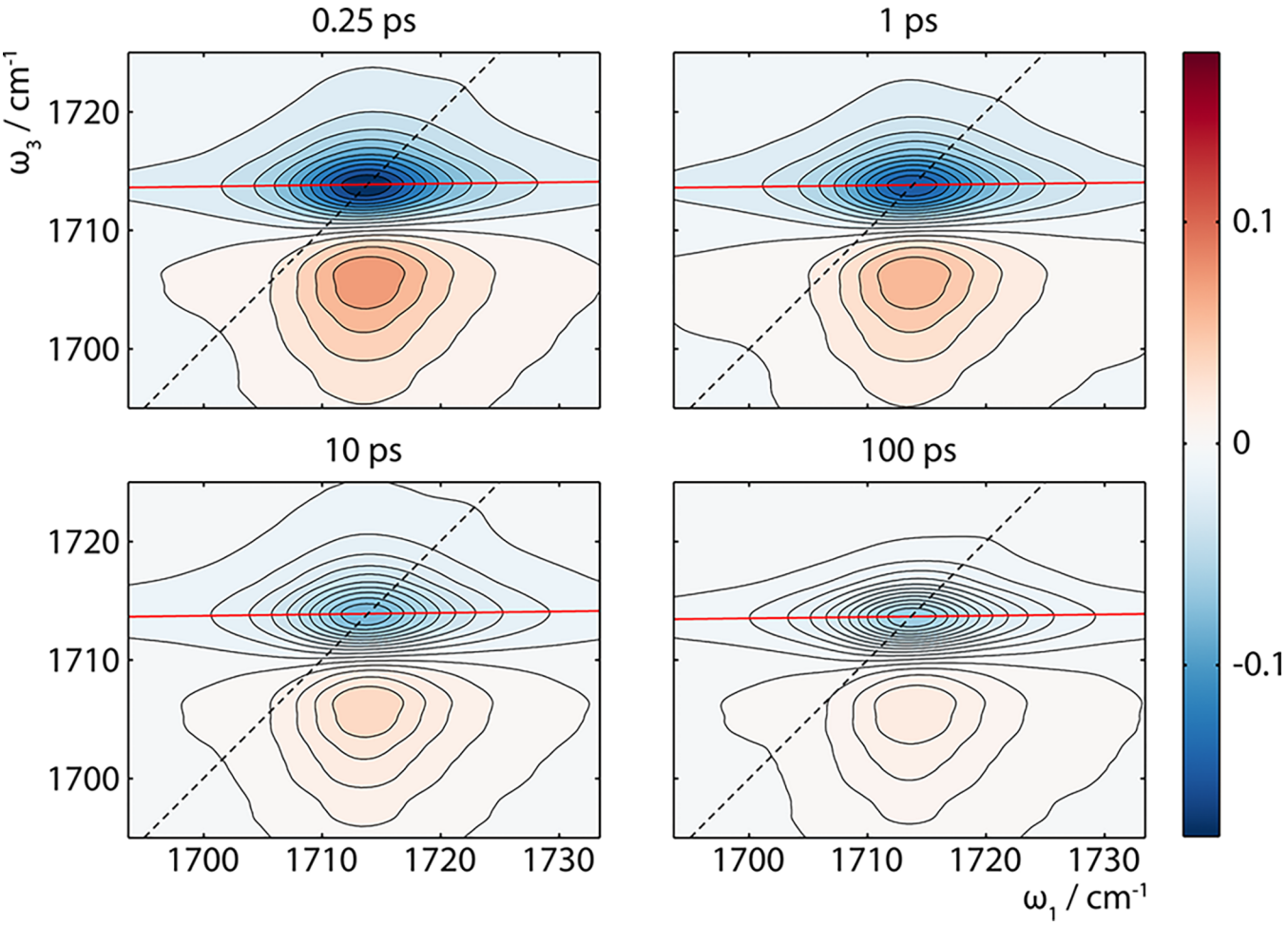

Figure 2. Isotropic 2DIR spectra of the C−N antisymmetric stretching vibration of FA^+ in $FAPbI_3$ thin films, for the four displayed waiting times. Fits to the GSB/SE center line slope are displayed in red, and black dashed lines mark the diagonal.

provide a possible explanation, however, this is unlikely given the long-lived component comprises 45% of the signal amplitude and the small surface-to-bulk ratio of the film. Some studies report the formation of water complexes around organic cations in perovskites,[36] but, given the care taken to use samples soon after synthesis, this seems unlikely. We rule out the presence of any δ-$FAPbI_3$ (yellow phase) in our samples based on absorbance measurements before and after ultrafast spectroscopic measurements, and our X-ray diffraction data. We conclude that our single value decomposition analysis is unable to fully remove the isotropic long-lived thermal heating component. However, comparisons of the isotropic response for different values of ω_3 in the SI (see Figure S5) shows that this does not significantly alter the 2.8 ps time constant.

The anisotropic response was calculated using the following relation:

$$R(t_2) = \frac{I_{para} - I_{perp}}{I_{para} + 2I_{perp}} \quad (2)$$

Figure 3b displays these data for the GSB/SE antisymmetric C−N stretching vibrational feature of each data set. These data were fit to a biexponential decay with an offset, which returned 470 ± 50 fs and 2.8 ± 0.5 ps time constants ($R^2 > 0.999$), with associated normalized exponential prefactors of 65% and 29%, and an offset corresponding to 6% of the total amplitude. We deduce that the long-time nonzero values of $R(t_2)$ arise from a small subensemble of the cation population that is unable to reorient, such as cations situated at the edges of crystals or at the film−substrate interface. We emphasize that this is a very minor (6%) component of the total population.

Snapshots of our 298 K molecular dynamics simulations (see SI for details) are given in Figure 4. They predict that the FA^+ cation preferentially orients $-NH_2$ groups toward opposing faces of cube formed by the Pb atoms. These observations are in agreement with a previous MD simulations[37] and time-averaged neutron diffraction studies.[38] For our room temperature MD simulations, we observe two key motions associated with the formamidinium cation (see animation of MD simulation in the SI): (i) the cation agitates around its mean position, but rotates around the axis formed by the two nitrogen atoms, and (ii) the cation undergoes a 90° jump about the center of the cube, such that the FA^+ $-NH_2$ groups point toward an adjacent pair of opposing cube faces (compare panels a and b in Figure 4). Our simulations also reveal that no part of the FA^+ cation remains fixed at the center of the cube. The autocorrelation function around the rotational axes that passes through the two nitrogen atoms was averaged over 83 trajectories, returning the ensemble rotational reorientation dynamics displayed in Figure 3c. Fits to these data return 680 ± 10 fs and 4.5 ± 0.1 ps time constants, which are in good numerical agreement with the values determined from the 2DIR anisotropy experiments. An animation illustrating the

DOI: 10.1021/acs.jpclett.7b03296
J. Phys. Chem. Lett. 2018, 9, 895−901

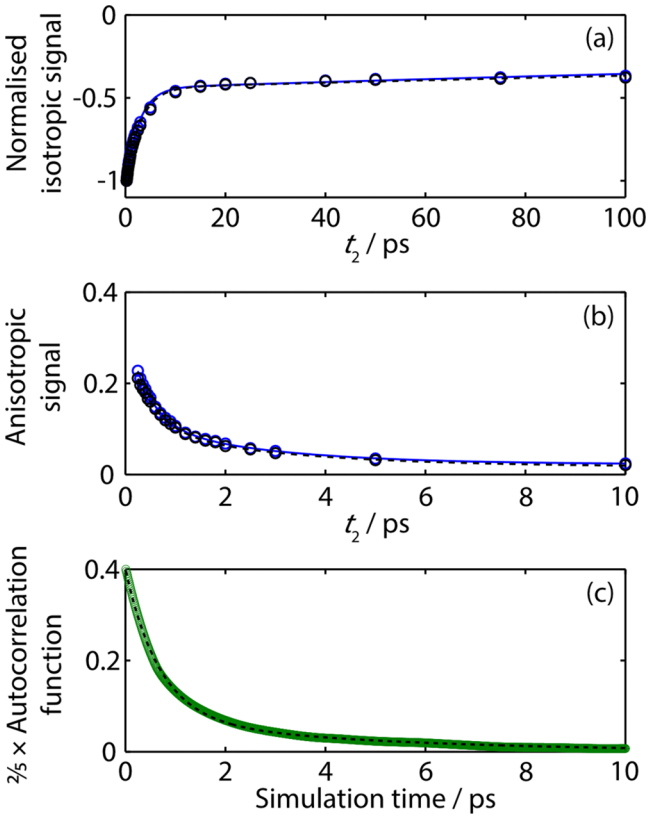

Figure 3. (a) Normalized population relaxation associated with the GSB/SE maxima for $FAPbI_3$ (blue circles) and $TiO_2/FAPbI_3$/Spiro-MeOTAD (black circles) with fits. (b) Anisotropy trace for the same feature between $0.25 \leq t_2 \leq 10$ ps. (c) Scaled autocorrelation response function returned by molecular dynamics simulations (green circles), and fit to the data in dashed black line.

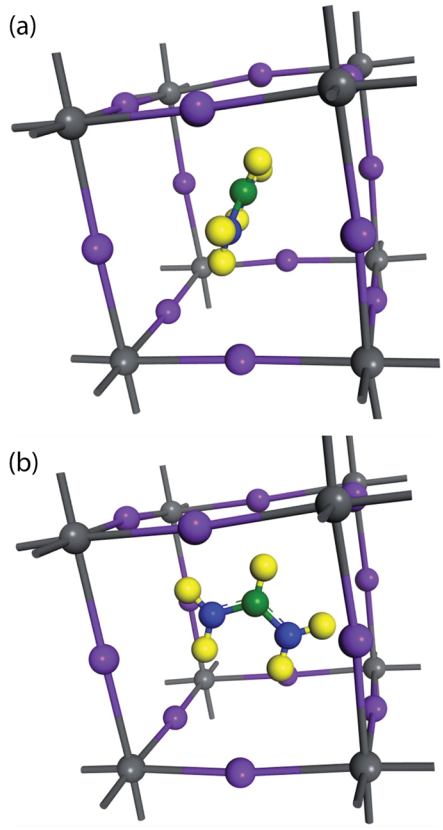

Figure 4. Representative snapshots from one cell of MD simulations highlighting the motions associated with a 90° flip between adjacent Pb cube faces.

FA^+ and lattice motions from MD simulation is included in the SI. We note that our MD simulations return different reorientation times compared to previous Born−Oppenheimer DFT-PBESOL MD simulations.[39] In our study, we have used classical MD simulations, and thus can afford to sample a far larger supercell ($8 \times 8 \times 8$) incorporating 512 FA^+ units. The force field used in our study accounts for effects of Pb/I ion dynamics and implements a Nośe−Hoover−Langevin thermostat. Both factors allow for a more realistic distribution of temperature fluctuations as expected for a canonical ensemble.

This distinctive two-part motion is reminiscent of the motions attributed to the MA^+ cation[12,14,19] in $MAPbI_3$, which used a coupled "wobbling in a cone/angular jump model" (equation given in SI) to fit the anisotropy data. Using this model to fit our experimental and MD simulations yield unrealistic parameters (see SI), and hence our data are fit to a generic biexponential decay function. We recognize that this diminishes our ability to directly attribute the two observed time constants to specific nuclear motions based on the 2DIR data alone. However, due to the good agreement between 2DIR anisotropy measurements and MD simulations, we can use the explicit motions observed in the MD simulations to assign the experimentally derived time constants.

Our 2DIR anisotropy measurements and MD simulations indicate that the barrier to rotational reorientation and sampling various faces of the lead-iodide lattice must be small relative to room temperature to explain the observed decay in $R(t_2)$ toward zero within 10 ps. This means, that the FA^+ moieties are unlikely to form ferroelectric domains with phenomenologically significant lifetimes, contrary to prior experimental and theoretical studies.[1,24,31,40] These observations explain the lack of spectral diffusion observed in our isotropic 2DIR line shapes; the vibrational dipole moment associated with the C−N antisymmetric stretch (see illustration inset in Figure 1a) will switch between adjacent and symmetric faces of a cube defined by the Pb atoms, leading to very similar intermolecular interactions. The transition between faces requires transit through an edge or corner of the cube; however, this is so rapid (see MD animation) that the vibrational potential is unaffected, thus explaining the minimal inhomogeneous broadening.

TRIR measurements, specifically near-IR pump and mid-infrared probe, were also performed for $FAPbI_3$ thin films to investigate the role of the formamidinium cations in the conduction band, or evidence for any vibration-intraband coupling. Results from our 760 nm pump, broadband mid-infrared probe (centered at 1725 cm^{-1}) experiments are displayed in Figure 5. Each TRIR spectra is dominated by two positive features; a sharp positive peak feature centered at 1718 cm^{-1}, attributed to a molecular vibration, and a broad diffuse feature that spans all probe frequencies. The latter has previously been assigned to electronic intraband transitions within the conduction band.[41,42] The sharp feature at 1718 cm^{-1} in our TRIR data has a similar line shape to the ground state FTIR spectrum (see Figure 1a), but is blue-shifted by 5 cm^{-1}, and notably has one-third the intensity of the intraband feature. Negative features at the ground state central frequency associated with the C−N antisymmetric stretching vibration are

DOI: 10.1021/acs.jpclett.7b03296
J. Phys. Chem. Lett. 2018, 9, 895−901

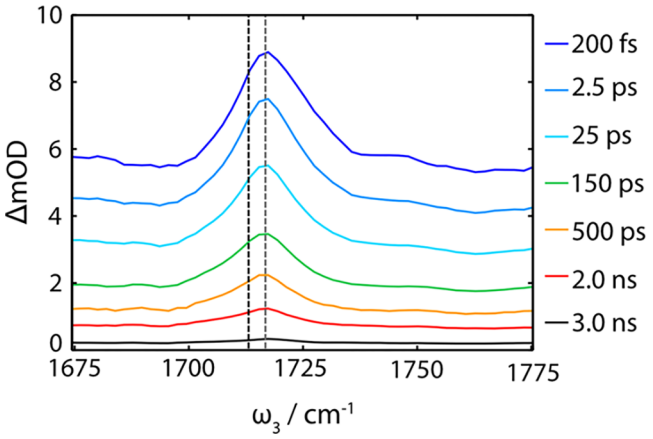

Figure 5. Time-resolved infrared studies for $FAPbI_3$ films using 760 nm (60 nJ) excitation and broadband mid-infrared probe for the displayed waiting times. The dashed black line marks ω_3 = 1713 cm^{-1}, the central frequency associated with the ground state FA^+ C−N antisymmetric stretching vibration; the dashed gray line helps highlight the central frequency of the transient vibrational feature (1718 cm^{-1}).

seemingly absent from our TRIR spectra, counter to our expectations based on typical TRIR line shapes (e.g., Figure S12a).

We rationalize these observations as follows: 760 nm pump photons generate charge-carriers either in the form of free carriers or polarons.[20,27,29,30] This results in an increased internal electric field in the perovskite thin film and changes the electrostatic environment surrounding FA^+ molecular cations compared to the valence band ground state. This nascent field perturbs the vibrational potential associated with the C−N antisymmetric stretching FA^+ vibration, and shifts the associated fundamental frequency, i.e. inducing a transient vibrational Stark shift. In addition, the vibrational transition dipole moment of the C−N antisymmetric stretch vibration in the conduction band must be enhanced significantly compared to the unperturbed vibration in the valence band. Such enhanced vibrational cross sections (termed infrared active vibrational (IRAV) modes) has been observed for thin polymer films, where the oscillator strength associated with vibrational transitions is enhanced by orders of magnitude, making them comparable to those typically associated with electronic states.[43−46] Consequentially, the positive transient feature dwarfs the negative feature in TRIR spectra (see Figure S12b). We note that in TRIR studies of $MAPbI_3$ films using nanosecond lasers,[42] the ratio of negative and positive transient signals are comparable, and reminiscent of a second derivative transient vibrational Stark line shape (see Figure S12a). We postulate this may be due to the time-delays examined in this study, i.e. > 10 ns, by which time a significant amount of charge-recombination will have occurred, leading to a reduced density of charge carriers/polarons in the film, and thus a diminished IRAV effect.

TRIR anisotropy experiments revealed no depolarization dynamics. Theoretical studies have demonstrated that FA^+ moieties do not participate in the Pb 6*p* ← I 5*p*/Pb 6*s* electronic transition,[47,48] and the molecular cation states do not contribute to the top of the valence or bottom of the conduction bands.[49,50] As our 2DIR results show, the FA^+ cations are not aligned in the bulk sample for any meaningful length of time. Consequentially, at t_2 = 0 fs there is no vector correlation between the electronic and vibrational transition dipole moments in question, and it is not possible to form a meaningful correlation function. One possible way to explore organic cation reorientation dynamics in the conduction band would be to perform transient-2DIR experiments.

A power-dependence TRIR study (30−120 nJ pump power) revealed the kinetics associated with the intraband were nonlinear, as per previous investigations.[51−53] Increasing the pump fluence generates an initial higher concentration of charge-carriers, which consequentially increases the probability of recombination, and thus leads to a concomitant reduction in conduction band lifetime. The power dependent TRIR data are provided in the SI.

To the best of our knowledge, this is the first direct experimental measurement of the rotational reorientation time scale for formamidinium cations in $FAPbI_3$, prior studies have inferred this from temperature dependent ^{15}N NMR, which has the potential to be sampling both α- and γ-$FAPbI_3$ phases,[54] or from MD calculations.[37,39] These studies put the cation reorientation time scale between 2 and 10 ps.[37,39,54] Our results indicate that the small-range motion of $FAPbI_3$ has a longer lifetime than those reported for $MAPbI_3$ (300 fs), but the larger "jump-like" motion occurs with the same frequency, within error. The differing lifetimes can be attributed to a complex interplay between the molecular cation physical structure, the bending modes of the FA^+ cation, and both $-NH_2$ groups producing stronger van der Waals interactions with the inorganic lattice (and therefore a larger activation barrier to rotation) than MA^+. The consistent "jump" lifetimes are somewhat surprising given the differing phase behavior of $MAPbI_3$ and $FAPbI_3$. It has been proposed that the organic cation rotation in $MAPbI_3$ is mediated by coupling to low-frequency phonon modes in the inorganic lattice, specifically those associated with octahedral titling and which contribute to $MAPbI_3$ phase transitions. From the phonon modes calculated by our calculations based on DFT-PBESOL linear response method, there are many phonon states with similar frequencies on the order of the cation rotational lifetimes (see Figure S14), and thus supports a model in which coupling to lattice phonon modes will be also important for FA^+ reorientation in $FAPbI_3$. In addition, we note that like MA^+ rotation in $MAPbI_3$,[12,14,55,56] these lifetimes are shorter than would be expected to facilitate the formation of sufficiently long-lived ferroelectric domains. Although, however unlikely it may seem, we cannot exclude the possibility of entire domains undergoing concerted interconversion on these time scales due to the ensemble nature of our measurements.

Two-dimensional infrared spectroscopy was used to determine 470 ± 50 fs and 2.8 ± 0.5 ps time constants for the rotational reorientation time scales associated with the formamidinium cation inside $FAPbI_3$ thin films. Complementary molecular dynamics simulations, relate these time constants with two FA^+ molecular motions: (i) an agitation around the center of the inorganic lattice and (ii) a 90° jump/flip between adjacent faces of the encapsulating lead cube. The picosecond component for FA^+ is remarkably similar to the value determined for methlyammonium cations inside $MAPbI_3$ thin films.[14] Our results rule out the existence of long-lived (anti)ferroelectric domains in $FAPbI_3$. Despite these similarities between cation dynamics, it is clear interactions with the inorganic lattice greatly vary with cation, and thus influence the material's bandgap. Based on our results, the observed power conversion efficiencies, and carrier recombination rates[1,57] of $FAPbI_3$ cannot be explained by (anti)ferroelectric domain

DOI: 10.1021/acs.jpclett.7b03296
J. Phys. Chem. Lett. 2018, 9, 895−901

formation, and are most likely explained by large polaron formation[29,58] or Rashba[9,22] splitting.

■ ASSOCIATED CONTENT

Supporting Information

The Supporting Information is available free of charge on the ACS Publications website at DOI: 10.1021/acs.jpclett.7b03296. All experimental data are archived in the University of Bristol's Research Data Storage Facility and are accessible using the doi: 10.5523/bris.2b3yc3iambhom2qypf31e3g4ov.

Details of the perovskite thin film synthesis and characterization using SEM and XRD; ultrafast 2DIR and TRIR experimental apparatus, 2DIR higher order singular value decomposition, and TRIR power studies; details of our CCSD and MD calculations (PDF)

Animation of the MD simulations (MPG)

■ AUTHOR INFORMATION

Corresponding Authors

*E-mail: tom.oliver@bristol.ac.uk.

*E-mail: d.tiwari@bristol.ac.uk.

ORCID

Victoria C. A. Taylor: 0000-0001-9495-8102

Paul M. Donaldson: 0000-0002-0305-9142

David J. Fermin: 0000-0002-0376-5506

Thomas A. A. Oliver: 0000-0003-3979-7857

Notes

The authors declare no competing financial interest.

■ ACKNOWLEDGMENTS

T.A.A.O. acknowledges financial support from the Royal Society through the award of a University Research Fellowship (UF1402310) and research grant (RG160046). D.J.F. and D.T. were supported by a PVTEAM programme grant (EP/L017792/1) awarded by the Engineering and Physical Sciences Research Council. V.C.A.T. and M.D. acknowledge Ph.D. studentships funded through BCFN (EP/G036780/1), and EPSRC DTA, respectively. Access to the LIFEtime system at the Central Laser Facility (of the UK STFC-Rutherford Appleton Laboratory) was awarded by STFC (Application 16230050). We thank the advanced Computing Research Centre, University of Bristol (www.bris.ac.uk/acrc/) for supercomputer time.

■ REFERENCES

(1) Zhumekenov, A. A.; Saidaminov, M. I.; Haque, M. A.; Alarousu, E.; Sarmah, S. P.; Murali, B.; Dursun, I.; Miao, X.-H.; Abdelhady, A. L.; Wu, T.; et al. Formamidinium Lead Halide Perovskite Crystals with Unprecedented Long Carrier Dynamics and Diffusion Length. *ACS Energy Lett.* **2016**, *1*, 32−37.

(2) Eperon, G. E.; Stranks, S. D.; Menelaou, C.; Johnston, M. B.; Herz, L. M.; Snaith, H. J. Formamidinium Lead Trihalide: a Broadly Tunable Perovskite for Efficient Planar Heterojunction Solar Cells. *Energy Environ. Sci.* **2014**, *7*, 982−987.

(3) Yin, W.-J.; Shi, T.; Yan, Y. Unique Properties of Halide Perovskites as Possible Origins of the Superior Solar Cell Performance. *Adv. Mater.* **2014**, *26*, 4653−4658.

(4) Steirer, K. X.; Schulz, P.; Teeter, G.; Stevanovic, V.; Yang, M.; Zhu, K.; Berry, J. J. Defect Tolerance in Methylammonium Lead Triiodide Perovskite. *ACS Energy Lett.* **2016**, *1*, 360−366.

(5) Wehrenfennig, C.; Liu, M.; Snaith, H. J.; Johnston, M. B.; Herz, L. M. Homogeneous Emission Line Broadening in the Organo Lead Halide Perovskite $CH_3NH_3PbI_{3-x}Cl_x$. *J. Phys. Chem. Lett.* **2014**, *5*, 1300−1306.

(6) Saidaminov, M. I.; Adinolfi, V.; Comin, R.; Abdelhady, A. L.; Peng, W.; Dursun, I.; Yuan, M.; Hoogland, S.; Sargent, E. H.; Bakr, O. M. Planar-Integrated Single-Crystalline Perovskite Photodetectors. *Nat. Commun.* **2015**, *6*, 8724.

(7) Stranks, S. D.; Snaith, H. J. Metal-Halide Perovskites for Photovoltaic and Light-Emitting Devices. *Nat. Nanotechnol.* **2015**, *10*, 391−402.

(8) Kagan, C. R.; Mitzi, D. B.; Dimitrakopoulos, C. D. Organic-Inorganic Hybrid Materials as Semiconducting Channels in Thin-Film Field-Effect Transistors. *Science* **1999**, *286*, 945−947.

(9) Kepenekian, M.; Robles, R.; Katan, C.; Sapori, D.; Pedesseau, L.; Even, J. Rashba and Dresselhaus Effects in Hybrid Organic−Inorganic Perovskites: From Basics to Devices. *ACS Nano* **2015**, *9*, 11557−11567.

(10) Brenner, T. M.; Egger, D. A.; Kronik, L.; Hodes, G.; Cahen, D. Hybrid Organic-Inorganic Perovskites: Low- Cost Semiconductors with Intriguing Charge- Transport Properties. *Nat. Rev. Mater.* **2016**, *1*, 15007.

(11) Ponseca, C. S., Jr.; Savenije, T. J.; Abdellah, M.; Zheng, K.; Yartsev, A.; Pascher, T.; Harlang, T.; Chabera, P.; Pullerits, T.; Stepanov, A.; et al. Organometal Halide Perovskite Solar Cell Materials Rationalized: Ultrafast Charge Generation, High and Microsecond-Long Balanced Mobilities, and Slow Recombination. *J. Am. Chem. Soc.* **2014**, *136*, 5189−5192.

(12) Selig, O.; Sadhanala, A.; Müller, C.; Lovrincic, R.; Chen, Z.; Rezus, Y. L. A.; Frost, J. M.; Jansen, T. L. C.; Bakulin, A. A. Organic Cation Rotation and Immobilization in Pure and Mixed Methylammonium Lead-Halide Perovskites. *J. Am. Chem. Soc.* **2017**, *139*, 4068−4074.

(13) Frost, J. M.; Whalley, L. D.; Walsh, A. Slow Cooling of Hot Polarons in Halide Perovskite Solar Cells. *ACS Energy Lett.* **2017**, *2*, 2647−2652.

(14) Bakulin, A. A.; Selig, O.; Bakker, H. J.; Rezus, Y. L. A.; Müller, C.; Glaser, T.; Lovrincic, R.; Sun, Z.; Chen, Z.; Walsh, A.; et al. Real-Time Observation of Organic Cation Reorientation in Methylammonium Lead Iodide Perovskites. *J. Phys. Chem. Lett.* **2015**, *6*, 3663−3669.

(15) Leguy, A. M. A.; Goñi, A. R.; Frost, J. M.; Skelton, J.; Brivio, F.; Rodríguez-Martínez, X.; Weber, O. J.; Pallipurath, A.; Alonso, M. I.; Campoy-Quiles, M.; et al. Dynamic Disorder, Phonon Lifetimes, and the Assignment of Modes to the Vibrational Spectra of Methylammonium Lead Halide Perovskites. *Phys. Chem. Chem. Phys.* **2016**, *18*, 27051−27066.

(16) Park, M.; Kornienko, N.; Reyes-Lillo, S. E.; Lai, M.; Neaton, J. B.; Yang, P.; Mathies, R. A. Critical Role of Methylammonium Librational Motion in Methylammonium Lead Iodide ($CH_3NH_3PbI_3$) Perovskite Photochemistry. *Nano Lett.* **2017**, *17*, 4151−4157.

(17) Beecher, A. N.; Semonin, O. E.; Skelton, J. M.; Frost, J. M.; Terban, M. W.; Zhai, H.; Alatas, A.; Owen, J. S.; Walsh, A.; Billinge, S. J. L. Direct Observation of Dynamic Symmetry Breaking Above Room Temperature in Methylammonium Lead Iodide Perovskite. *ACS Energy Lett.* **2016**, *1*, 880−887.

(18) Haruyama, J.; Sodeyama, K.; Han, L.; Tateyama, Y. First-Principles Study of Ion Diffusion in Perovskite Solar Cell Sensitizers. *J. Am. Chem. Soc.* **2015**, *137*, 10048−10051.

(19) Leguy, A. M. A.; Frost, J. M.; McMahon, A. P.; Sakai, V. G.; Kochelmann, W.; Law, C.; Li, X.; Foglia, F.; Walsh, A.; Regan, B. C. O. R.; et al. The Dynamics of Methylammonium Ions in Hybrid Organic-Inorganic Perovskite Solar Cells. *Nat. Commun.* **2015**, *6*, 7124.

(20) Zhu, X. Y.; Podzorov, V. Charge Carriers in Hybrid Organic−Inorganic Lead Halide Perovskites Might Be Protected as Large Polarons. *J. Phys. Chem. Lett.* **2015**, *6*, 4758−4761.

(21) Lee, J.-H.; Bristowe, N. C.; Lee, J. H.; Lee, S.-H.; Bristowe, P. D.; Cheetham, A. K.; Jang, H. M. Resolving the Physical Origin of Octahedral Tilting in Halide Perovskites. *Chem. Mater.* **2016**, *28*, 4259−4266.

(22) Etienne, T.; Mosconi, E.; De Angelis, F. Dynamical Origin of the Rashba Effect in Organohalide Lead Perovskites: a Key to Suppressed Carrier Recombination in Perovskite Solar Cells? *J. Phys. Chem. Lett.* **2016**, *7*, 1638−1645.
(23) Motta, C.; El-Mellouhi, F.; Kais, S.; Tabet, N.; Alharbi, F.; Sanvito, S. Revealing the Role of Organic Cations in Hybrid Halide Perovskite $CH_3NH_3PbI_3$. *Nat. Commun.* **2015**, *6*, 7026.
(24) Frost, J. M.; Walsh, A. What Is Moving in Hybrid Halide Perovskite Solar Cells? *Acc. Chem. Res.* **2016**, *49*, 528−535.
(25) Filip, M. R.; Eperon, G. E.; Snaith, H. J.; Giustino, F. Steric Engineering of Metal-Halide Perovskites with Tunable Optical Band Gaps. *Nat. Commun.* **2014**, *5*, 5757.
(26) Green, M. A.; Jiang, Y.; Soufiani, A. M.; Ho-Baillie, A. Optical Properties of Photovoltaic Organic−Inorganic Lead Halide Perovskites. *J. Phys. Chem. Lett.* **2015**, *6*, 4774−4785.
(27) Amat, A.; Mosconi, E.; Ronca, E.; Quarti, C.; Umari, P.; Nazeeruddin, M. K.; Grätzel, M.; De Angelis, F. Cation-Induced Band-Gap Tuning in Organohalide Perovskites: Interplay of Spin−Orbit Coupling and Octahedra Tilting. *Nano Lett.* **2014**, *14*, 3608−3616.
(28) Frost, J. M.; Butler, K. T.; Brivio, F.; Hendon, C. H.; van Schilfgaarde, M.; Walsh, A. Atomistic Origins of High-Performance in Hybrid Halide Perovskite Solar Cells. *Nano Lett.* **2014**, *14*, 2584−2590.
(29) Neukirch, A. J.; Nie, W.; Blancon, J.-C.; Appavoo, K.; Tsai, H.; Sfeir, M. Y.; Katan, C.; Pedesseau, L.; Even, J.; Crochet, J. J.; et al. Polaron Stabilization by Cooperative Lattice Distortion and Cation Rotations in Hybrid Perovskite Materials. *Nano Lett.* **2016**, *16*, 3809−3816.
(30) Wright, A. D.; Verdi, C.; Milot, R. L.; Eperon, G. E.; Perez-Osorio, M. A.; Snaith, H. J.; Giustino, F.; Johnston, M. B.; Herz, L. M. Electron-Phonon Coupling in Hybrid Lead Halide Perovskites. *Nat. Commun.* **2016**, *7*, 11755.
(31) Quarti, C.; Mosconi, E.; De Angelis, F. Structural and Electronic Properties of Organo-Halide Hybrid Perovskites From Ab Initio Molecular Dynamics. *Phys. Chem. Chem. Phys.* **2015**, *17*, 9394−9409.
(32) Liu, S.; Zheng, F.; Koocher, N. Z.; Takenaka, H.; Wang, F.; Rappe, A. M. Ferroelectric Domain Wall Induced Band Gap Reduction and Charge Separation in Organometal Halide Perovskites. *J. Phys. Chem. Lett.* **2015**, *6*, 693−699.
(33) Galkowski, K.; Mitioglu, A.; Miyata, A.; Plochocka, P.; Portugall, O.; Eperon, G. E.; Wang, J. T.-W.; Stergiopoulos, T.; Stranks, S. D.; Snaith, H. J.; et al. Determination of the Exciton Binding Energy and Effective Masses for Methylammonium and Formamidinium Lead Tri-Halide Perovskite Semiconductors. *Energy Environ. Sci.* **2016**, *9*, 962−970.
(34) Zhou, Z.; Pang, S.; Ji, F.; Zhang, B.; Cui, G. The Fabrication of Formamidinium Lead Iodide Perovskite Thin Films via Organic Cation Exchange. *Chem. Commun.* **2016**, *52*, 3828−3831.
(35) Hills-Kimball, K.; Nagaoka, Y.; Cao, C.; Chaykovsky, E.; Chen, O. Synthesis of Formamidinium Lead Halide Perovskite Nanocrystals Through Solid−Liquid−Solid Cation Exchange. *J. Mater. Chem. C* **2017**, *5*, 5680−5684.
(36) Christians, J. A.; Miranda Herrera, P. A.; Kamat, P. V. Transformation of the Excited State and Photovoltaic Efficiency of $CH_3NH_3PbI_3$ Perovskite Upon Controlled Exposure to Humidified Air. *J. Am. Chem. Soc.* **2015**, *137*, 1530−1538.
(37) Carignano, M. A.; Saeed, Y.; Aravindh, S. A.; Roqan, I. S.; Even, J.; Katan, C. A Close Examination of the Structure and Dynamics of $HC(NH_2)_2PbI_3$ by MD Simulations and Group Theory. *Phys. Chem. Chem. Phys.* **2016**, *18*, 27109−27118.
(38) Weller, M. T.; Weber, O. J.; Henry, P. F.; Di Pumpo, A. M.; Hansen, T. C. Complete Structure and Cation Orientation in the Perovskite Photovoltaic Methylammonium Lead Iodide Between 100 and 352 K. *Chem. Commun.* **2015**, *51*, 4180−4183.
(39) Weller, M. T.; Weber, O. J.; Frost, J. M.; Walsh, A. Cubic Perovskite Structure of Black Formamidinium Lead Iodide, α-$[HC(NH_2)_2]PbI_3$, at 298 K. *J. Phys. Chem. Lett.* **2015**, *6*, 3209−3212.
(40) Walsh, A. Principles of Chemical Bonding and Band Gap Engineering in Hybrid Organic−Inorganic Halide Perovskites. *J. Phys. Chem. C* **2015**, *119*, 5755−5760.
(41) Sauvage, S.; Boucaud, P.; Julien, F. H.; Gérard, J. M.; Marzin, J. Y. Infrared Spectroscopy of Intraband Transitions in Self-Organized InAs/GaAs Quantum Dots. *J. Appl. Phys.* **1997**, *82*, 3396−3401.
(42) Narra, S.; Chung, C.-C.; Diau, E. W.-G.; Shigeto, S. Simultaneous Observation of an Intraband Transition and Distinct Transient Species in the Infrared Region for Perovskite Solar Cells. *J. Phys. Chem. Lett.* **2016**, *7*, 2450−2455.
(43) Heeger, A. J.; Kivelson, S.; Schrieffer, J. R.; Su, W. P. Solitons in Conducting Polymers. *Rev. Mod. Phys.* **1988**, *60*, 781−850.
(44) Miranda, P. B.; Moses, D.; Heeger, A. J. Ultrafast Photogeneration of Charged Polarons in Conjugated Polymers. *Phys. Rev. B: Condens. Matter Mater. Phys.* **2001**, *64*, 1182−1184.
(45) Sakamoto, A.; Nakamura, O.; Tasumi, M. Picosecond Time-Resolved Polarized Infrared Spectroscopic Study of Photoexcited States and Their Dynamics in Oriented Poly(*p*-Phenylenevinylene). *J. Phys. Chem. B* **2008**, *112*, 16437−16444.
(46) Chin, X. Y.; Yin, J.; Wang, Z.; Caironi, M.; Soci, C. Mapping Polarons in Polymer FETs by Charge Modulation Microscopy in the Mid-Infrared. *Sci. Rep.* **2015**, *4*, 839−6.
(47) Kim, J.; Lee, S.-C.; Lee, S.-H.; Hong, K.-H. Importance of Orbital Interactions in Determining Electronic Band Structures of Organo-Lead Iodide. *J. Phys. Chem. C* **2015**, *119*, 4627−4634.
(48) Ma, J.; Wang, L.-W. Nanoscale Charge Localization Induced by Random Orientations of Organic Molecules in Hybrid Perovskite $CH_3NH_3PbI_3$. *Nano Lett.* **2015**, *15*, 248−253.
(49) Borriello, I.; Cantele, G.; Ninno, D. Ab Initio investigation of Hybrid Organic-Inorganic Perovskites Based on Tin Halides. *Phys. Rev. B: Condens. Matter Mater. Phys.* **2008**, *77*, 235214.
(50) Brivio, F.; Walker, A. B.; Walsh, A. Structural and Electronic Properties of Hybrid Perovskites for High-Efficiency Thin-Film Photovoltaics From First-Principles. *APL Mater.* **2013**, *1*, 042111−042116.
(51) Piatkowski, P.; Cohen, B.; Kazim, S.; Ahmad, S.; Douhal, A. How Photon Pump Fluence Changes the Charge Carrier Relaxation Mechanism in an Organic-Inorganic Hybrid Lead Triiodide Perovskite. *Phys. Chem. Chem. Phys.* **2016**, *18*, 27090−27101.
(52) Manser, J. S.; Kamat, P. V. Band Filling with Free Charge Carriers in Organonietal Halide Perovskites. *Nat. Photonics* **2014**, *8*, 737−743.
(53) Kudriashova, L. G.; Kiermasch, D.; Rieder, P.; Campbell, M.; Tvingstedt, K.; Baumann, A.; Astakhov, G. V.; Dyakonov, V. Impact of Interfaces and Laser Repetition Rate on Photocarrier Dynamics in Lead Halide Perovskites. *J. Phys. Chem. Lett.* **2017**, *8*, 4698−4703.
(54) Kubicki, D. J.; Prochowicz, D.; Hofstetter, A.; Zakeeruddin, S. M.; Grätzel, M.; Emsley, L. Phase Segregation in Cs-, Rb- and K-Doped Mixed-Cation $(MA)_X(FA)_{1-x}PbI_3$ Hybrid Perovskites From Solid-State NMR. *J. Am. Chem. Soc.* **2017**, *139*, 14173−14180.
(55) Zhu, H.; Miyata, K.; Fu, Y.; Wang, J.; Joshi, P. P.; Niesner, D.; Williams, K. W.; Jin, S.; Zhu, X. Y. Screening in Crystalline Liquids Protects Energetic Carriers in Hybrid Perovskites. *Science* **2016**, *353*, 1409−1413.
(56) Gélvez-Rueda, M. C.; Cao, D. H.; Patwardhan, S.; Renaud, N.; Stoumpos, C. C.; Schatz, G. C.; Hupp, J. T.; Farha, O. K.; Savenije, T. J.; Kanatzidis, M. G.; et al. Effect of Cation Rotation on Charge Dynamics in Hybrid Lead Halide Perovskites. *J. Phys. Chem. C* **2016**, *120*, 16577−16585.
(57) Han, Q.; Bae, S.-H.; Sun, P.; Hsieh, Y.-T.; Yang, Y. M.; Rim, Y. S.; Zhao, H.; Chen, Q.; Shi, W.; Li, G.; et al. Single Crystal Formamidinium Lead Iodide $(FAPbI_3)$: Insight Into the Structural, Optical, and Electrical Properties. *Adv. Mater.* **2016**, *28*, 2253−2258.
(58) Sendner, M.; Nayak, P. K.; Egger, D. A.; Beck, S.; Muller, C.; Epding, B.; Kowalsky, W.; Kronik, L.; Snaith, H. J.; Pucci, A.; et al. Optical Phonons in Methylammonium Lead Halide Perovskites and Implications for Charge Transport. *Mater. Horiz.* **2016**, *3*, 613−620.

DOI: 10.1021/acs.jpclett.7b03296
J. Phys. Chem. Lett. 2018, 9, 895−901